Sintering and crystallization behavior of CaMgSi 2 O 6 – NaFeSi 2 O 6 based glass-ceramics

Ashutosh Goel, Anna Maria Ferrari, Ishu Kansal, Maria J. Pascual, Luisa Barbieri, Federica Bondioli, Isabella Lancellotti, Manuel J. Ribeiro, and José M. F. Ferreira

Citation: Journal of Applied Physics **106**, 093502 (2009); doi: 10.1063/1.3239852
View online: http://dx.doi.org/10.1063/1.3239852
View Table of Contents: http://scitation.aip.org/content/aip/journal/jap/106/9?ver=pdfcov
Published by the AIP Publishing

Sintering and crystallization behavior of $CaMgSi_2O_6-NaFeSi_2O_6$ based glass-ceramics

Ashutosh Goel,[1,2] Anna Maria Ferrari,[3] Ishu Kansal,[1,2] Maria J. Pascual,[4] Luisa Barbieri,[2] Federica Bondioli,[2] Isabella Lancellotti,[2] Manuel J. Ribeiro,[5] and José M. F. Ferreira[1,a)]
[1]*Department of Ceramics and Glass Engineering, CICECO, University of Aveiro, 3810-193 Aveiro, Portugal*
[2]*Dipartimento di Ingegneria dei Materiali e dell'Ambiente, Facoltà di Ingegneria, Universitá di Modena e Reggio Emilia, 41100 Modena, Italy*
[3]*Dipartimento di Scienze e Metodi dell'Ingegneria, Facoltà di Ingegneria, Universitdiá Modena e Reggio Emilia, 42100 Reggio Emilia, Italy*
[4]*Instituto de Cerámica y Vidrio, CSIC, Kelsen 5, Campus de Cantoblanco, 28049 Madrid, Spain*
[5]*UIDM, ESTG, Polytechnic Institute of Viana do Castelo, 4900 Viana do Castelo, Portugal*

(Received 5 June 2009; accepted 31 August 2009; published online 4 November 2009)

We report on the synthesis, sintering, and crystallization behaviors of a glass with a composition corresponding to 90 mol % $CaMgSi_2O_6-10$ mol % $NaFeSi_2O_6$. The investigated glass composition crystallized superficially immediately after casting of the melt and needs a high cooling rate (rapid quenching) in order to produce an amorphous glass. Differential thermal analysis and hot-stage microscopy were employed to investigate the glass forming ability, sintering behavior, relative nucleation rate, and crystallization behavior of the glass composition. The crystalline phase assemblage in the glass-ceramics was studied under nonisothermal heating conditions in the temperature range of 850–950 °C in both air and N_2 atmosphere. X-ray diffraction studies adjoined with the Rietveld–reference intensity ratio method were employed to quantify the amount of crystalline phases, while electron microscopy was used to shed some light on the microstructure of the resultant glass-ceramics. Well sintered glass-ceramics with diopside as the primary crystalline phase were obtained where the amount of diopside varied with the heating conditions. © *2009 American Institute of Physics*. [doi:10.1063/1.3239852]

I. INTRODUCTION

The pyroxenes are a group of important rock forming silicate minerals found in many igneous and metamorphic rocks. They are silicates that, in their simplest form, contain single SiO_3 chains of linked SiO_4 tetrahedra. Generally, a small amount of Si is replaced by Al and other small cations. The name "pyroxene" is derived from the Greek words for *fire* and *stranger*. They have been named this way because of their presence in volcanic lavas, where they are sometimes seen as crystals embedded in volcanic glass. They were considered to be impurities in the glass, hence the name "fire strangers." The general chemical formula for pyroxenes is $M2M1T_2O_6$, where $M2$ refers to cations in a generally distorted octahedral coordination (Mg^{2+}, Fe^{2+}, Mn^{2+}, Li^{+}, $Ca2^{+}$, and Na^{2+}), $M1$ refers to cations in a regular octahedral coordination (Al^{3+}, Fe^{3+}, Ti^{4+}, Cr^{3+}, V^{3+}, Ti^{3+}, Zr^{4+}, Sc^{3+}, Zn^{2+}, Mg^{2+}, Fe^{2+}, and Mn^{2+}), and T refers to tetrahedrally coordinated cations (Si^{4+}, Al^{3+}, and Fe^{3+}).[1]

Pyroxenes belong to either the orthorhombic or the monoclinic crystal systems. Monoclinic pyroxenes are called clinopyroxenes. Their space groups are $C2/c$, $P21/c$, and $P2/n$, depending on their chemical composition and petrogenetic history. The chain silicate structure of the pyroxenes offers much flexibility in the incorporation of various cations, and the names of the pyroxene minerals are primarily defined by their chemical composition. The stability of clinopyroxenes over a broad spectrum of chemical compositions, in conjunction with the possibility of achieving desired physical properties and high chemical durability, has generated worldwide interest due to their possible use in different technological applications, for example, biomedicine,[2–5] fuel cells,[6,7] nuclear waste immobilization,[8,9] and electrical insulators.[10,11] Despite the interesting features and practical applications as mentioned above, the literature survey reveals that clinopyroxene based ceramics have received less attention and hence poor documentation in literature.

Diopside belongs to the group of inosilicates, and it is an important member of the clinopyroxene group with the composition $CaMgSi_2O_6$. The stoichiometric diopside glasses and resultant glass-ceramics have been investigated by many researchers for several properties and mechanisms due to their wide applicability in different practical applications.[12–14] In our previous studies, we have investigated the development of glasses and glass-ceramics along the diopside-Ca-Tschermak join.[15–17] It has been reported that all the compositions exhibit good glass forming ability and sinterability, and the solubility limit of Ca-Tschermak in diopside is about 30 mol %.

Recently, diopside based ceramics and glass-ceramics have generated significant interest in the scientific community due to their potential application as bioactive materials. Nonami and Tsutsumi[3] fabricated a composite of diopside and hydroxyapatite (HAp) in order to increase the fracture toughness of pure sintered HAp. It was shown that the bending strength and fracture toughness of the diopside-HAp

a)Author to whom correspondence should be addressed. Tel.: +351-234-370242. FAX: +351-234-370204. Electronic mail: jmf@ua.pt.

composite was two to three times higher in comparison to sintered HAp. Further, it was revealed that diopside has no general toxicity in cell cultures, and it helps in bone regeneration. Similarly, De Aza *et al.*[4] soaked diopside based ceramic pellets in human parotid saliva over different time intervals to investigate the behavior of the material in a natural medium of high protein content. The results showed the formation of the HAp layer on the surface of the ceramic and suggested that the mechanism of the HAp layer formation in saliva was similar to that showed in *in vitro* tests by other silica based materials.

Yoganand *et al.*[18] developed bioactive glass-ceramics with a transferred arc plasma technique in the system $CaO-MgO-SiO_2$ with diopside as the major crystalline phase. HAp formation on the glass-ceramic surface was observed after 12 days of immersion in simulated body fluid (SBF), while fibroblast culture results showed that the glass-ceramics were nontoxic to human fibroblasts and promoted cell growth. It has been reported that the glass-ceramic system with a eutectic composition of 38 wt % tricalcium phosphate (TCP) $(3CaO \cdot P_2O_5) \cdot 62$ wt % diopside shows a flexural strength of more than 200 MPa.[19] Unfortunately, the bioactivity of this material was not reported. Kamitakahara *et al.*[20] synthesized porous glass-ceramics containing TCP and diopside, evaluated their bioactivity by examining the *in vitro* apatite formation in SBF, and proposed the porous glass-ceramics as scaffold materials for bone repair.

In the light of the above mentioned perspective, we have investigated a new diopside $(CaMgSi_2O_6)$—aegirine $(NaFeSi_2O_6)$ based glass-ceramic composition for its potential application as bioactive glass-ceramic in hyperthermia treatment. Since it has been reported that Na_2O-free glass-ceramics in the system $CaO-SiO_2-FeO-Fe_2O_3$ do not exhibit bioactivity[21] and considering the excellent bioactive properties of diopside as reported in literature, we have formulated a glass composition with a theoretical 90 mol % diopside −10 mol % aegirine ratio. Similar to diopside, aegirine is also a member of the clinopyroxene family. However, no study pertaining to aegirine based glass-ceramics has been reported so far. In a series of papers, the present paper will focus on the synthesis, sintering, and crystallization behavior of the parent glass, while the forthcoming articles will report on the structural, magnetic, and bioactive properties of its derivative glasses and resultant glass-ceramics. As reported by Kokubo *et al.*[22] that the apatite formation ability (*in vitro*) of a bioactive glass-ceramic comes from the resultant glassy phase, therefore, the present study will focus on the quantification of various crystalline phases and the remaining amorphous phase in the glass-ceramics by the Rietveld–reference intensity ratio (RIR) method.[23]

II. EXPERIMENTAL

A. Glass preparation

A glass with the theoretical composition 16.64 MgO −23.15 CaO−1.42 Na_2O−3.66 Fe_2O_3 −55.12 SiO_2 (wt %), corresponding to the general formula $Ca_{0.9}Mg_{0.9}Na_{0.1}Fe_{0.1}Si_2O_6$, was prepared in bulk and frit form by the conventional melt-quenching technique. Powders of technical grade SiO_2 (purity > 99.5%) and $CaCO_3$ (>99.5%) and of reactive grade Fe_2O_3 (Baker and Adamson, NJ, purity > 99.0%), $MgCO_3$ (BDH Chemicals Ltd., UK, purity > 99.0%), and Na_2CO_3 (Sigma Aldrich, Portugal, purity > 99.0%) were used. Homogeneous mixtures of batches (~100 g), obtained by ball milling, were preheated at 900 °C for 1 h for calcination and then melted in Pt crucibles at 1580 °C for 1 h in air. Glasses in bulk form were produced by pouring the melts on preheated bronze molds followed by annealing at 550 °C for 1 h. The experimental composition of glass was determined by inductive coupled plasma–optical emission spectroscopy (ICP-OES) (Jobin Yvon, JY 70 plus, France). The results from ICP-OES of the experimental glass did not reveal any significant changes relative to the theoretical composition except a small decrease in MgO. The samples of the glass powder compacts were produced from glass frits, which were obtained by quenching of glass melts in cold water. The mean particle size of the glass powder used in the present study ranged from 10 to 15 μm (determined by the light scattering technique; Coulter LS 230, Beckman Coulter, Fullerton CA; Fraunhofer optical model).

B. Thermal analysis

The differential thermal analysis (DTA) (Netzsch 402 EP, Germany) of fine powder was carried out in air from room temperature to 1050 °C at heating rates (β) of 2, 5, 10, and 20 K min^{-1}. The values of the glass transition temperature (midpoint of the endothermic dip) T_g, crystallization onset temperature T_c, and peak temperature of crystallization T_p were also determined. In order to calculate the nucleation rate, the glass powder was subjected to heating at different temperatures in the vicinity of the suspected nucleation maxima (between T_g and T_c) for 30 min. The peak temperatures associated with respective crystallization exotherms reflect the variations in nucleation rates.

The sintering behavior of the glass sample was investigated by using a hot-stage microscope (HSM). A side-view HSM EM 201 equipped with an image analysis system and electrical furnace 1750/15 Leica was used. The microscope projects the image of the sample through a quartz window and onto the recording device. The computerized image analysis system automatically records and analyzes the geometry changes of the sample during heating. The image analyzer takes into account the thermal expansion of the alumina substrate while measuring the height of the sample during firing, with the base as a reference. The HSM software calculates the percentage of decrease in height, width, and area of the sample images. The measurements were conducted in air with a heating rate of 5 K min^{-1}. The cylindrical shaped samples with height and diameter of ≈3 mm were prepared by cold-pressing the glass powders. The cylindrical samples were placed on a $10 \times 15 \times 1$ mm^3 alumina (>99.5 wt % Al_2O_3) support. The temperature was measured with a Pt/Rh (6/30) thermocouple contacted under the alumina support. The temperatures corresponding to the characteristic viscosity points (first shrinkage, maximum

shrinkage, softening, half ball, and flow) were obtained from the photographs taken during the hot-stage microscopy experiment following Scholze's definition[24] and Ref. 25.

C. Crystallization of glass powder compacts

Round shaped pellets with a 20 mm diameter and an ~3 mm thickness were prepared from fine glass powder by uniaxial pressing (80 MPa). The samples were sintered under nonisothermal conditions for 1 h at 850, 900, and 950 °C in a tubular furnace in air and N_2 atmosphere. The experiments were conducted in two different atmospheres (air and N_2) in order to investigate their effect on crystalline phase assemblage in the resultant glass-ceramics and their magnetic properties (will be published in a forthcoming article) as it is well known that heat treatment in N_2 atmosphere can prevent the formation of nonmagnetic phases.[26] A slow heating rate of 2 K min^{-1} was maintained in order to prevent the deformation of the samples.

The linear shrinkage during sintering was calculated from the difference of the diameter between the green and the sintered pellets, while the apparent density of glass-ceramics was obtained by using the Archimedes principle (immersion of pellets in di-ethyl phthalate). The mean values and the standard deviations presented for linear shrinkage and density have been obtained from (at least) ten different samples.

D. Mineralogical characterization

The amorphous nature of the glasses, along with a qualitative and quantitative analysis of crystalline phases in the glass-ceramics (crushed to particle size <25 μm), was determined by the x-ray diffraction (XRD) analysis using a conventional Bragg–Brentano diffractometer (Philips PW 3710, Eindhoven, The Netherlands) with Ni-filtered Cu $K\alpha$ radiation. The quantitative phase analysis of the glass-ceramics was made by the combined Rietveld-RIR method. A 10 wt % of corundum (NIST SRM 674a, annealed at 1500 °C for 1 day to increase the crystallinity to 100%) was added to all the glass-ceramic samples as an internal standard. The mixtures, ground in an agate mortar, were side loaded in an aluminum flat holder in order to minimize the preferred orientation problems. Data were recorded in 2θ range=5–140° (step size of 0.02° and 6 s of counting time for each step). The phase fractions were extracted by Rietveld-RIR refinements using GSAS software[27] and EXPGUI (Ref. 28) as a graphical interface and were rescaled on the basis of the absolute weight of corundum originally added to their mixtures as an internal standard and, therefore, internally renormalized. The background was successfully fitted with a Chebyshev function with a variable number of coefficients depending on its complexity. The peak profiles were modeled using a pseudo-Voigt function with one Gaussian and one Lorentzian coefficient. Lattice constants, phase fractions, and coefficients corresponding to sample displacement and asymmetry were also refined.

Microstructural observations were done on polished (mirror finishing) as well as fractured samples. The as obtained glass and the etched glass-ceramic samples (by immersion in a 2 vol % HF solution for a duration of 2 min and by washing with distilled water in order to stop the etching process and avoid the fluoride formation) were observed by scanning electron microscopy (SEM) (SU-70, Hitachi) with energy dispersive spectroscopy (EDS) (Bruker Quantax, Germany) to study the distribution of elements in the crystals.

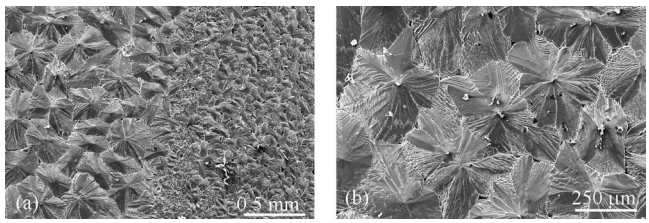

FIG. 1. SEM image of the crystallized layer of glass (fractured surface).

III. RESULTS AND DISCUSSION

A. Glass forming ability

The glass composition was prone for easy casting after 1 h of soaking time at 1580 °C, resulting in homogeneous and transparent frits with brown color (probably due to Fe_2O_3). The amorphous nature of the quenched frits was confirmed by XRD analysis. On the contrary, it was difficult to produce a stable bulk glass as the surface of a glass rod, which was in direct contact with air (and not in contact with metallic mold) crystallized immediately after pouring the melt on the bronze mold, while the remaining part of the sample did not show any tendency toward crystallization. The microstructure of the crystallized layer reveals the presence of uniformly grown crystals of two different sizes with a rosette-like morphology (Fig. 1). XRD and EDS mapping of these crystals exhibit the formation of diopside ($CaMgSi_2O_6$; ICDD: 01-078-1390) and magnesium iron oxide ($Mg_{1.55}Fe_{1.6}O_4$; ICDD: 01-080-0073) on the surface of the glass. The tendency toward crystallization of glass during casting implies the need for rapid quenching of glasses based on diopside-aegirine compositions.

No diopside based glass compositions, as investigated in our previous studies,[6,7,15–17] were prone to crystallization during the casting of the melt; therefore, in quest of the reason for lower glass forming tendency of the investigated glass, we investigated its kinetic fragility (F) index using DTA. The kinetic fragility index (F) is a measure of the rate at which the relaxation time decreases with increasing temperature around T_g and is given by the following equation:[29]

$$F = \frac{E_\eta}{RT_g \ln 10}, \tag{1}$$

where R is the universal gas constant, E_η is referred to as the activation energy of viscous flow occurring around glass transition, which is further calculated by the following equation:[30]

$$\ln\left(\frac{T_g^2}{\beta}\right) = \frac{E_\eta}{RT_g} + \text{const.} \tag{2}$$

The DTA curves of the glass powder heated at different heating rates (Fig. 2) exhibit an inflection before the onset of

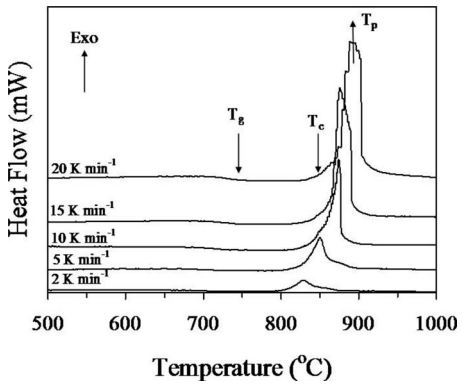

FIG. 2. DTA thermographs of the fine glass powder at different heating rates.

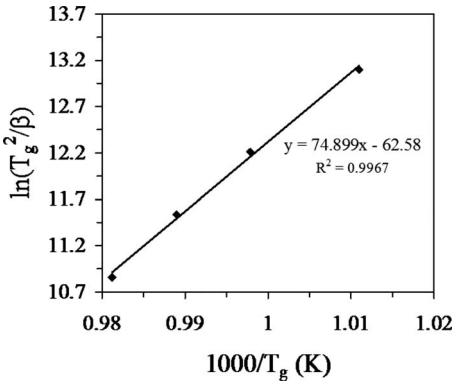

FIG. 3. Plot for the determination of the activation energy of viscous flow (E_η) for the investigated glass composition.

crystallization (T_c), representing glass transition temperature (T_g). The value of T_g was observed to be 729 °C at the heating rate of 5 K min^{-1} (Table I) and shifted toward the higher side with an increase in heating rate. The value of E_η, as calculated from Eq. (2) (Fig. 3) and listed in Table I, is much higher than our previously investigated diopside based glasses.[31] It has already been reported by various researchers that E_η is responsible for the molecular motion, and the rearrangement of the atoms around T_g and the glass with the lowest activation energy value is the most stable one.[32] Therefore, a higher E_η value implies a thermal instability of the investigated glass composition. Furthermore, the F value, as obtained from Eq. (1) and reported in Table I, is much higher in comparison to diopside-Ca-Tschermak based glass, as reported in our previous study.[31] According to Vilgis,[33] glass forming liquids that exhibit an approximate Arrhenius temperature dependence of their relaxation times are defined as strong and specified with a low value of F ($F \approx 16$), while the limit for fragile glass forming liquids is characterized by a high value of F ($F \approx 200$).[34] In the present investigation, since the value of F is much lower than 200, a stable glass could be obtained by a rapid quenching of the melt in water or by placing the melt in contact with the metallic mold. However, due to the higher value of F in comparison to its other diopside based counterparts,[31] the investigated glass showed a poor glass forming ability and surface crystallization during the casting of the melt.

TABLE I. Thermal parameters obtained from DTA and HSM for glass at β=5 K min^{-1}.

T_g (°C)	729 ± 2
E_η (kJ mol^{-1})	623 ± 3
F	32.36 ± 0.42
T_{FS} (°C)	750 ± 5
T_{MS} (°C)	810 ± 5
T_c (°C)	812 ± 2
T_p (°C)	850 ± 2
T_{HB} [a] (°C)	1326 ± 5
T_F [b] (°C)	1342 ± 2
A/A_0	0.67

[a] T_{HB}: temperature for half ball formation.
[b] T_F: flow temperature.

B. Sintering and crystallization behaviors by HSM and DTA

During the sintering of a glass powder compact with a wide grain size distribution, small particles get sintered first, as shown by Prado *et al.*[35] Thus, sintering kinetics at the first shrinkage is dominated by the neck formation among the smallest particles by viscous flow and is best described by the Frenkel model of sintering.[36] The maximum shrinkage is reached when larger pores (pores formed from cavities among larger particles) have disappeared due to viscous flow that reduces their radii with time. This region of sintering kinetics may be described by the Mackenzie–Shuttleworth model of sintering.[37] However, various physical processes (entrapped insoluble gases, crystallization) occurring at the very end of the sintering process might affect the densification kinetics. A comparison between DTA and HSM results under the same heating conditions can be useful in investigating the effect of glass composition on sintering and devitrification phenomena. In general, two different trends can be observed related to the sintering and crystallization behaviors of the glasses.[25] In the first case, the beginning of crystallization (T_c) occurs after the final sintering stage. Thus, under such circumstances, sintering and crystallization are independent processes. However, in the other case, T_c appears before maximum density has been reached. In this case, the crystallization process starts before a complete densification, thus preventing further sintering.

The variation in the relative area and heat flow with respect to temperature as obtained from HSM and DTA, respectively, for the investigated glass composition at a heating rate of 5 K min^{-1} is presented in Fig. 4. In particular, photomicrographs presented in Fig. 5 show changes in the geometric shape of the glass powder compact with respect to temperatures obtained from HSM. In the present study, sintering started at temperatures much lower than the onset of crystallization, thus resulting in a well sintered glass-ceramic. Table I lists the characteristic temperatures for the glass as obtained by DTA (T_g, T_c, and T_p) and HSM (T_{FS}, T_{MS}, T_{HB}, and T_F). A/A_0 corresponds to the ratio of the final area/initial area of the glass powder compact. In the present case, even though the onset of crystallization occurred nearly at T_{MS} (Fig. 4), the A/A_0 value of 0.67 at T_{MS} (as presented in Table I) implies good densification (95%–98%).[25] In the

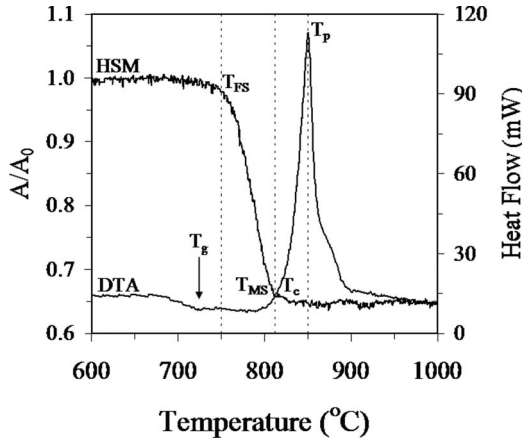

FIG. 4. Comparison of DTA and HSM curves on the same temperature scale for the investigated glass composition at a heating rate of 5 K min^{-1}.

present study, sintering started (T_{FS}) at a temperature lower than other diopside based glass systems as reported in our previous studies.[38,39] However, the sinterability parameter, as defined by $T_c - T_{MS}$,[25] reflecting the sintering behavior of the glass composition is quiet low. It is evident that the investigated glass composition, even if well sintered, showed poorer sintering ability in comparison to its other diopside based counterparts.[6,7] Furthermore, since the densification of glass powder compacts is initially obtained through viscous flow at temperatures slightly higher than T_g, the activation energy of viscous flow (E_η) plays a crucial role in defining the sintering behavior of the glass composition. In the present case, the value of E_η=623 kJ mol^{-1} is much higher in comparison to Al_2O_3 containing diopside-Ca-Tschermak glass compositions.[31] Therefore, a low sintering ability can be expected for the diopside-aegirine glass composition.

The DTA plot of glass exhibits single exothermic effects (Fig. 2) at all the heating rates, which shifted toward higher temperatures with increasing heating rate. This signifies that the glass-ceramic is formed as a result either of single phase crystallization or of an almost simultaneous precipitation of different crystalline phases. The T_p value of 850 °C obtained for the investigated glass heated at 5 K min^{-1} is much lower than the values presented by other diopside based glasses.[31,38,39] This difference can be attributed to the net-

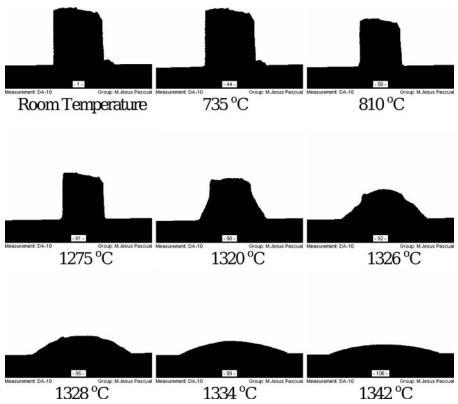

FIG. 5. HSM images of glass on an alumina substrate at various stages of heating cycle.

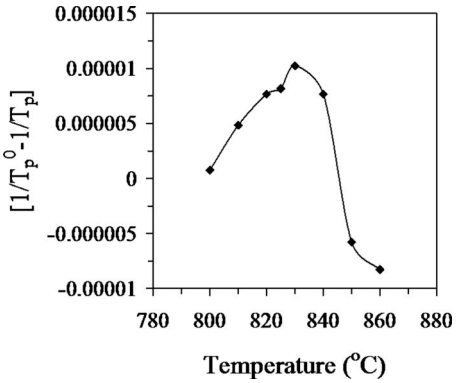

FIG. 6. Marotta method results for the investigated glass composition. The quantity on the *y*-axis is proportional to the logarithm of the nucleation rate [Eq. (3)].

work modifier effect of Na_2O and to the nucleating effect of Fe_2O_3 unlike the network forming effect of Al_2O_3.[17]

The relative nucleation rates for the investigated glass composition were calculated using the following equation:[40,41]

$$\ln(I_0) = \frac{E_c}{R}\left(\frac{1}{T_p^0} - \frac{1}{T_p}\right) + \text{const}, \tag{3}$$

where I_0 is the steady state nucleation rate, E_c is the activation energy for crystal growth, and T_p and T_p^0 are peak temperatures without and with an intermediate nucleation thermal hold, respectively. Plotting $(1/T_p^0 - 1/T_p)$ versus

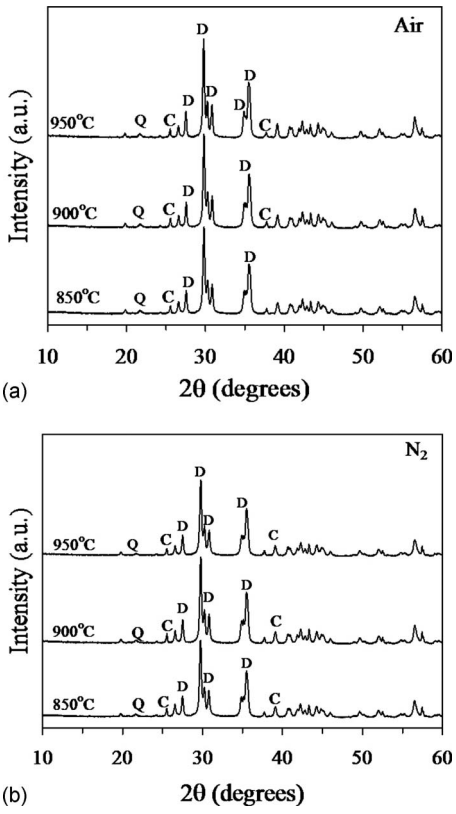

FIG. 7. X-ray diffractograms of glass powder compacts sintered at 850, 900, and 950 °C for 1 h in (a) air and (b) N_2 atmosphere (D: diopside, Q: low quartz, and C: corundum). Spectra are not normalized. Full intensity: 60 000 cps.

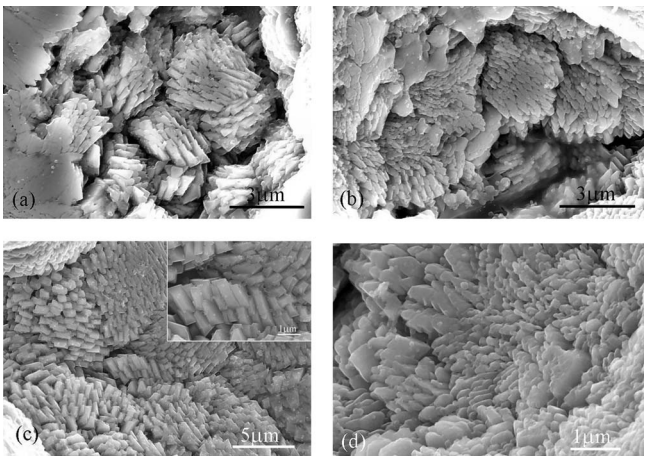

FIG. 8. SEM images of GCs sintered at (a) 850 °C in air, (b) 900 °C in air, (c) 900 °C in N_2, and (d) 950 °C in N_2.

intermediate hold temperatures produces a nucleation-rate-like curve (Fig. 6), which shows that maximum nucleation in this sample occurs at around 830 °C, while a sharp decrease in nucleation rate can be observed with an increase in temperature from 830 to 850 °C. The constant term in Eq. (3) indicates that this technique does not provide absolute nucleation rates, but only relative ones.

C. Crystallization of glass powder compacts

In agreement with HSM and DTA results, well sintered glass powder compacts were obtained after heat treatment of powder compacts in the temperature range of 850–950 °C for 1 h both in air and N_2 atmosphere, respectively. Figure 7 presents XRD diffractograms of the glass powder compacts after heat treatment in air [Fig. 7(a)] and N_2 atmosphere [Fig. 7(b)]. The qualitative analysis shows that diopside ($CaMgSi_2O_6$; ICDD card 078-1390; ICSD card 62545) precipitates as the main crystalline phase along with minor traces of low quartz (SiO_2; ICDD card 085-0460; ICSD card 16334) in all the glass powder compacts heat treated between 850 and 950 °C. In agreement with XRD results, no significant differences could be observed in the microstructure of glass-ceramics (Fig. 8) treated at different temperatures and in two different atmospheres. The SEM images presented in Fig. 8 depict the presence of well crystallized and densely packed diopside crystals in all the glass-ceramics. The quantitative analysis by the Rietveld-RIR analysis (Fig. 9, Table II) reveals that all the resultant glass-ceramics have a high degree of crystallization (glassy phase: 10%–40%).[13] Figure 9 shows the refinement of a glass-ceramic powder compact fired at 950 °C in N_2 atmosphere. The crystallinity in the glass-ceramics decreases with an increase in temperature from 850 to 900 °C, irrespective of the atmosphere, while it increases with further increase in temperature to 950 °C. Furthermore, at any temperature, the amount of crystallinity in the samples, sintered in air atmosphere, was higher in comparison to those sintered in N_2. Similar results were revealed by the linear shrinkage and density measurements of the glass-ceramic powder compacts (Fig. 10). The linear shrinkage and density values were higher for glass powder compacts sintered in air in comparison to those sintered in N_2 atmosphere (Fig. 10), thus confirming the results of quan-

TABLE II. Results of Rietveld-RIR quantitative analysis (wt %).

Phases	850 °C	900 °C	950 °C
	In air		
Diopside	86.5 (2)	70.9 (3)	85.4 (2)
Quartz	0.5 (5)	0.5 (4)	0.5 (5)
Glass	13.0 (7)	28.6 (7)	14.1 (7)
Total	100	100	100
χ^2	4.41	4.44	4.71
R_{wp}	0.052	0.051	0.053
R_p	0.039	0.039	0.039
	In N_2		
Diopside	75.1 (3)	68.0 (3)	78.9 (2)
Quartz	0.5 (5)	0.5 (4)	0.4 (5)
Glass	24.4 (8)	31.5 (7)	20.7 (7)
Total	100	100	100
χ^2	4.12	4.60	3.67
R_{wp}	0.050	0.052	0.048
R_p	0.038	0.039	0.037

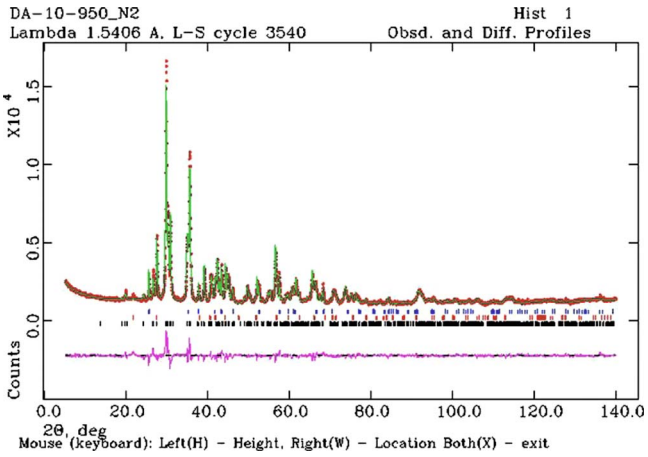

FIG. 9. (Color online) Observed (crosses), calculated (continuous line), and difference curve from the Rietveld refinement of the GC sample treated at 950 °C for 1 h in air. Markers representing the phase reflections correspond to corundum, quartz, and diopside (from top to bottom).

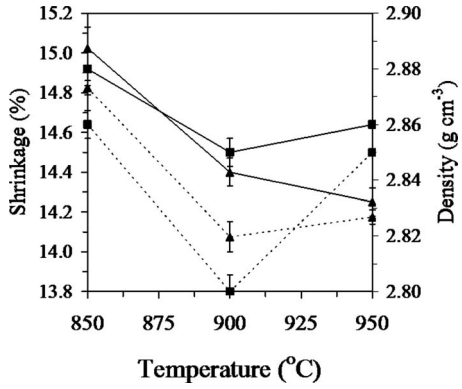

FIG. 10. Influence of temperature and atmosphere on density and linear shrinkage of the sintered GCs. ▲ represents shrinkage, while ■ represents density; bold lines correspond to air atmosphere, while broken lines correspond to N_2 atmosphere.

titative analysis. Also, in accordance with the amount of crystalline content in the glass-ceramics, the density of the glass-ceramics was calculated to be highest at 850 °C, while it lowers with a decrease in crystalline content at 900 °C and further increases at 950 °C (Fig. 10). Since the potential bioactivity of diopside is a proven fact,[3,4] one can expect higher bioactivity from the glass-ceramics with >70 wt % diopside. However, the absence of magnetic crystalline phases in the investigated glass-ceramic samples (both in air and N_2) implies a need for increasing aegirine content in the glass-ceramics in order to obtain suitable magnetic properties for hyperthermia treatment. This will be focused upon in our future work.

IV. CONCLUSIONS

A glass composition with the general formula $Ca_{0.9}Mg_{0.9}Na_{0.1}Fe_{0.1}Si_2O_6$ was prepared and investigated for its glass forming ability along with sintering and crystallization behaviors. There is a good agreement between theoretical and experimental results pertaining to the glass forming and crystallization abilities of the investigated glass. The glass composition was prone to crystallization, immediately after casting of the melt, and therefore needed rapid quenching in order to obtain an amorphous and transparent glass. A good sintering behavior was observed for the glass composition, resulting in the formation of dense glass-ceramics with diopside as the major crystalline phase. The nucleation maxima occurred at ~830 °C, and the relative nucleation rate decreased considerably with further increase in temperature. As revealed by a quantitative analysis, the amount of diopside was higher in glass-ceramics sintered in air atmosphere in comparison to N_2 atmosphere. The presence of ≥70 wt % diopside qualifies these glass-ceramics for further experimentation as potential bioactive materials for hyperthermia treatment. However, there is still a need to increase the Fe content in the glasses in order to obtained magnetic crystalline phases.

In the light of the results obtained in the present investigation, the future work will be focused on increasing the glass forming ability of these glass compositions, designing new compositions with higher $NaFeSi_2O_6$ content and evaluation of magnetic as well as bioactive properties of the resultant glass-ceramics.

ACKNOWLEDGMENTS

This study was financially supported by the University of Aveiro, CICECO, and FCT, Portugal (Grant No. SFRH/BD/37037/2007).

[1]N. Morimoto, Can. Mineral. **27**, 143 (1989).
[2]D. U. Tulyaganov and R. Ya. Khodakovskaya, Glass Ceram. **48**, 221 (1991).
[3]T. Nonami and S. Tsutsumi, J. Mater. Sci.: Mater. Med. **10**, 475 (1999).
[4]P. N. De Aza, Z. B. Luklinska, and M. Anseau, J. Biomed. Mater. Res., Part B: Appl. Biomater. **73B**, 54 (2005).
[5]W. Xue, C. Ding, C. Cao, and Y. Dong, Key Eng. Mater. **288–289**, 319 (2005).
[6]A. Goel, D. U. Tulyaganov, V. V. Kharton, A. A. Yaremchenko, S. Eriksson, and J. M. F. Ferreira, J. Power Sources **189**, 1032 (2009).
[7]A. Goel, D. U. Tulyaganov, V. V. Kharton, A. A. Yaremchenko, and J. M. F. Ferreira, Acta Mater. **56**, 3065 (2008).
[8]I. W. Donald, B. L. Metcalfe, and R. N. J. Taylor, J. Mater. Sci. **32**, 5851 (1997).
[9]I. W. Donald, Eur. J. Glass Sci. Technol. A **48**, 155 (2007).
[10]W. Höland and G. N. Beall, *Glass-Ceramic Technology* (Wiley-Blackwell, Westerville, OH, 2002).
[11]W. E. Lee and A. H. Heuer, J. Am. Ceram. Soc. **70**, 349 (1987).
[12]M. L. F. Nascimento, E. B. Ferreira, and E. D. Zanotto, J. Chem. Phys. **121**, 8924 (2004).
[13]L. Barbieri, F. Bondioli, I. Lancellotti, C. Leonelli, M. Montorsi, and A. M. Ferrari, J. Am. Ceram. Soc. **88**, 3131 (2005).
[14]S. Reinsch, M. L. F. Nascimento, R. Müller, and E. D. Zanotto, J. Non-Cryst. Solids **354**, 5386 (2008).
[15]A. Goel, D. U. Tulyaganov, S. Agathopoulos, M. J. Ribeiro, R. N. Basu, and J. M. F. Ferreira, J. Eur. Ceram. Soc. **27**, 2325 (2007).
[16]A. Goel, D. U. Tulyaganov, S. Agathopoulos, M. J. Ribeiro, and J. M. F. Ferreira, J. Eur. Ceram. Soc. **27**, 3231 (2007).
[17]A. Goel, E. R. Shaaban, D. U. Tulyaganov, and J. M. F. Ferreira, J. Am. Ceram. Soc. **91**, 2690 (2008).
[18]C. P. Yoganand, V. Selvarajan, L. Lusvarghi, O. M. Goudouri, K. M. Paraskevopoulos, and M. Rouabhia, Mater. Sci. Eng., C **29**, 1759 (2009).
[19]M. Ashizuka and E. Ishida, J. Mater. Sci. **32**, 185 (1997).
[20]M. Kamitakahara, C. Ohtsuki, K. Yuko, S.-I. Ogata, M. Tanihara, and T. Miyazaki, J. Ceram. Soc. Jpn. **114**, 82 (2006).
[21]Y. Ebisawa, F. Miyaji, T. Kokubo, K. Ohura, and T. Nakamura, Biomaterials **18**, 1277 (1997).
[22]T. Kokubo, H. Kusitani, C. Ohtsuki, S. Sakka, and Y. Yamamuro, J. Mater. Sci.: Mater. Med. **3**, 79 (1992).
[23]A. F. Gualtieri and G. Artioli, Powder Diffr. **10**, 269 (1995).
[24]H. Scholze, Dtsch Ver. Keram. Ges. **391**, 63 (1962).
[25]M. J. Pascual, A. Durán, and M. O. Prado, Phys. Chem. Glasses **46**, 512 (2005).
[26]R. P. del Real, D. Arcos, and M. Vallet-Regí, Chem. Mater. **14**, 64 (2002).
[27]A. C. Larson and R. B. von Dreele, General Structure Analysis System (GSAS), LANSCE Report No. MS-H805, Los Alamos National Laboratory, Los Alamos, NM, 1998.
[28]B. H. Toby, J. Appl. Crystallogr. **34**, 210 (2001).
[29]M. M. Wakkad, E. Kh. Shokr, and S. H. Mohamed, J. Non-Cryst. Solids **265**, 157 (2000).
[30]S. Mahadevan, A. Giridhar, and A. K. Singh, J. Non-Cryst. Solids **88**, 11 (1986).
[31]A. Goel, D. U. Tulyaganov, E. R. Shaaban, R. N. Basu, and J. M. F. Ferreira, J. Appl. Phys. **104**, 043529 (2008).
[32]O. A. Lafi, M. M. A. Imran, and M. K. Abdullah, Physica B **395**, 69 (2007).
[33]T. A. Vilgis, Phys. Rev. B **47**, 2882 (1993).
[34]R. Bohmer and C. A. Angell, in *Disorder Effects on Relaxation Processes*, edited by R. Richert and A. Blumen (Springer, Berlin, 1994).
[35]M. O. Prado, E. D. Zanotto, and R. Muller, J. Non-Cryst. Solids **279**, 169 (2001).
[36]J. Frenkel, J. Phys. (USSR) **9**, 385 (1945).
[37]J. K. Mackenzie and R. Shuttleworth, Proc. Phys. Soc. London **62**, 833 (1949).
[38]A. Goel, D. U. Tulyaganov, M. J. Pascual, E. R. Shaaban, F. Munoz, Z. Lu, and J. M. F. Ferreira, J. Non-Cryst. Solids (unpublished).
[39]A. Goel, D. U. Tulyaganov, A. M. Ferrari, E. R. Shaaban, A. Prange, F. Bondioli, and J. M. F. Ferreira, J. Am. Ceram. Soc. (unpublished).
[40]A. Marotta, A. Buri, and F. Branda, J. Mater. Sci. **16**, 341 (1981).
[41]A. Marotta, A. Buri, F. Branda, and S. Saiello, in *Nucleation and Crystallization in Glasses*, Advances in Ceramics Vol. 4, edited by J. H. Simmons, D. R. Uhlmann, and G. H. Beall (American Ceramic Society, Columbus, OH, 1982), pp. 146–152.